

A *XMM*-Newton observation of a sample of four close dSph galaxies.

Manni L.^{1,2}, Nucita A.A.^{1,2}, De Paolis F.^{1,2}, Testa V.³, Ingrosso G.^{1,2}

¹*Department of Mathematics and Physics “E. De Giorgi”, University of Salento, Via per Arnesano, CP 193, I-73100, Lecce, Italy*

²*INFN, Sez. di Lecce, Via per Arnesano, CP 193, I-73100, Lecce, Italy*

³*INAF, Osservatorio Astronomico di Roma, via di Frascati 33, 00040 Monteporzio, Italy*

Accepted xxx; Received xxx; in original form xxx

ABSTRACT

We present the results of the analysis of deep archival *XMM*-Newton observations towards the dwarf spheroidal galaxies Draco, Leo I, Ursa Major II and Ursa Minor in the Milky Way neighbourhood. The X-ray source population is characterized and cross-correlated with available databases with the aim to infer their nature. We also investigate if intermediate-mass black holes are hosted in the center of these galaxies.

In the case of Draco, we detect 96 high-energy sources, two of them being possibly local stars, while no evidence for any X-ray emitting central compact object is found.

Towards the Leo I and UMa II field of view we reveal 116 and 49 X-ray sources, respectively. None of them correlates with the putative central black holes and only one is likely associated with a UMa II local source.

The study of the UMi dwarf galaxy shows 54 high-energy sources and a possible association with a source at the dSph center. We put an upper limit to the central compact object luminosity of 4.02×10^{33} erg/s. Furthermore, via the correlation with a radio source near the galactic center, we get that the putative black hole should have a mass of $(2.76^{+32.00}_{-2.54}) \times 10^6 M_{\odot}$ and be radiatively inefficient. This confirms a previous result obtained by using Chandra data alone.

Key words: X–rays: individual: Draco dSph - Leo I dSph - UMa II dSph - UMi dSph - black hole physics

1 INTRODUCTION

Dwarf spheroidal galaxies (dSphs) are very peculiar star systems with mass in the range $10^3 - 10^7 M_{\odot}$ (Martin et al. 2008) and relatively poor in stars. Consequently they result very faint and difficult to be detected and studied in details. In the past decades, the interest in dSphs has rapidly grown up. Indeed, until 2001, only 9 Milky Way (MW) dwarf satellites (at distance between 16 and 250 kpc) were known (Odenkirchen et al. 2001) while, recently, McConnachie (2012) listed over 100 nearby galaxies in and around the Local Group, along with their relevant physical properties.

If dSphs orbit close enough to the Galactic center, they may lose mass and be disrupted by the tidal forces due to the Galactic potential. Tidal effects can be easily revealed in the Sagittarius dSph which has a peculiar shape characterized by stellar debris along its orbit (see Mateo et al. 1998, Ibata et al. 2001). Tidal extension signatures for Carina and Ursa Minor dSphs were also detected by Majewski et al. (2000) and Martinez-Delgado et al. (2001). On the contrary, Odenkirchen et al. (2001) showed that there is no evidence for the existence of a tail-like extension of the Draco dSph star population beyond its tidal radius.

dSph are characterized by large mass-to-light ratios. This leads scientists to infer that they are dark matter (DM) dominated objects (see e.g. Mateo 1997). Breddels & Helmi (2013) performed

a comparison between different dSph formation scenarios using a sample of DM profiles and argued that no particular model is significantly preferred among others. Moreover, some authors suggest different dSph growing processes, without contemplating DM content. In this respect, Yang et al. (2014), by using numerical simulations, claim that a merger in M31, occurred 8.5 Gyr ago, could have ejected a tidal-tail toward our direction. So that, dSph could be generated from the interaction between the low-mass tidal dwarf galaxies and our MW.

As far as the origin and evolution of dSphs, they can be either remnants of bigger systems, disrupted by tidal forces or affected by supernova winds that take out the overwhelming majority of gas (Silk et al. 1987), or small mass systems since their origin. In the latter case, they could be the building blocks of large galaxies (with mass in the range $10^9 - 10^{11} M_{\odot}$) while, in the absence of interaction (merging or disruption), they can survive until now. To address these issues, dSphs are nowadays intensively studied by numerical simulations to infer their formation and evolution (Assmann et al. 2013a, Assmann et al. 2013b, Casas et al. 2012).

Additionally, as globular clusters, dSphs host old stellar populations and, consequently, X-ray sources are expected to be most likely low mass X-ray binaries (LMXBs) or cataclysmic variables (CVs). However, one fundamental difference between globular clusters and dSphs is their central stellar density that can be at

least two order of magnitude smaller in dSphs (Harris (1996); McConnachie (2012)). Then, at variance with globular clusters where it is thought that the high stellar density forms a nursery for LMXB through capture, in the case of dSphs any X-ray binary should be primordial. However, due to the old stellar population, LMXBs would turn off in a few hundred million years, making unlikely finding these systems in dSphs.

The lower stellar density of dSph offers a contrasting environment with respect to that in globular clusters and a comparison of the X-ray source populations in the two cases may help testing the LMXB formation scenario. This is exactly the case of the Sculptor dSph which was studied by Maccarone et al. (2005b) who found five X-ray sources (likely X-ray binaries with a neutron star or a black hole primary) with $L_X \geq 6 \times 10^{33} \text{ erg s}^{-1}$ associated to the galaxy. This discovery, from one side proves that LMXBs can exist in a old stellar environment with low stellar encounters. From the other side, it is clearly challenging for the LMXB formation theory.

Hence, one of the goals of this paper is to attempt a classification of the X-ray sources identified towards our dSph sample and pinpoint local (or candidate local) sources. Detecting X-ray sources in dSph can, moreover, help in the investigation of the dark matter component in these objects. Indeed, when neutron stars form in SN II explosions they get large kick velocities ($\sim 100 \text{ km s}^{-1}$, Podsiadlowski et al. 2004) exceeding the escape local velocity (a few km s^{-1}) due to the stellar component of the dSph. However, if dSphs have a dark matter halo, LMXBs (and even isolated millisecond pulsars which are direct descendant of LMXBs) can be retained within the galaxy (Dehnen & King 2006).

dSphs are also the best candidates to host intermediate mass black holes (hereinafter IMBHs) in their gravitational cores. This clue derives by extrapolating fundamental $M_{BH} - M_{Bulge}$ relation (see e.g. Magorrian et al. 1998, for the super massive BH case) down to the typical dSph masses. In particular, IMBH masses can be evaluated either via dynamical considerations or using the fundamental plane relation at radio and X-ray wavelengths (see e.g., Reines et al. 2013, Nucita et al. 2013a, Nucita et al. 2013b). We also mention that, within the galaxy hierarchy scenario, IMBHs may be the ground seeds for the formation of super massive BHs hosted in the center of galaxies.

Searches for IMBHs in dSphs have been attempted recently. In a very interesting paper, Lemons et al. (2015) have analyzed a sample of ≈ 44000 dSph galaxies detected by the Sloan Digital Sky Survey (SDSS) with redshift $z \leq 0.055$ and stellar mass content $M_* \leq 3 \times 10^9 M_\odot$. By a cross-correlation with the Chandra Source Catalogue, it was found that 19 galaxies have at least a detectable hard X-ray source within three half light radii. Moreover, for about half of this sample, there is the evidence that the X-ray source (possibly a massive black hole candidate) is associated to the optical nucleus of the dSph. Of course, as pointed out by the authors, follow-up observations are necessary to disentangle between stellar-mass X-ray binaries and the existence of active galactic nuclei with an accreting BH as central engine.

On the basis of these results, we also searched in the selected dSphs for X-ray sources with the typical signatures of accreting IMBHs. Although the statistics at hand is low, it is interesting that we find fraction of galaxies in our sample that appear hosting a central X-ray source is similar to that observed by Lemons et al. (2015). Also in our case, only dedicated follow-up observations may allow to unveil the source nature.

The paper is structured as follows: in Section 2 we briefly describe the sample of objects used in our study. Section 3 presents the procedure used to analyze the *XMM*-Newton data. The results

for the high-energy study of dSphs are reported in Section 4 and, finally, in Section 5 we address our conclusions.

2 DSPH SAMPLE

Our study is concerned with the high-energy characterization of dSphs. We select the dSph sample for which *XMM*-Newton archival data are available. We did not consider the Fornax dSph galaxy since it was already studied in details by Orio et al. (2010) and Nucita et al. (2013a). Here, we remind that these authors found an X-ray source possibly associated to a variable star belonging to the galaxy and two more sources at the boundaries of the Fornax globular clusters GC 3 and GC 4. Furthermore, following Jardel & Gebhardt (2012) who predicted the existence of a central IMBH with mass $\approx 3 \times 10^4 M_\odot$, Nucita et al. (2013a) searched also for X-ray targets at the galaxy center. In the particular case of one of the possible gravitational centers reported in Stetson et al. (1998), the authors found a close X-ray source. The source unabsorbed 0.2–12 keV flux is $3 \times 10^{-15} \text{ erg s}^{-1} \text{ cm}^{-2}$ corresponding to an intrinsic luminosity of $L_X \approx 7 \times 10^{33} \text{ erg s}^{-1}$ (assuming a galaxy distance of 138 kpc): in the IMBH hypothesis (and assuming a Bondi spherycal accretion or in the context of a Keplerian thin disk model), the compact object seems to accrete very inefficiently.

In this paper, we focus our attention on four galaxies¹: Draco, Leo I, Ursa Major II and Ursa Minor (hereafter UMa II and UMi, respectively).

2.1 Draco

The Draco dSph (at J2000 coordinates $RA = 17^h 20^m 12.4^s$ and $Dec = 57^\circ 54' 55''$) is a MW companion galaxy. Since its discovery (Wilson 1955) this galaxy became target of many observational campaigns. Baade & Swope (1961) first derived the distance to the galaxy to be about 99 kpc through the identification of variable stars. In addition, others studies on Draco variables were made by Zinn & Searle (1976), Nemec (1985), Goranskij (1982), Kinemuchi et al. (2002) and Bonanos et al. (2004). Recently, Kinemuchi et al. (2008) presented a survey with the photometry of different kind of sources (270 RR Lyrae stars, 9 anomalous Cepheids, 2 eclipsing binaries, 12 slow irregular red variables, 30 background QSOs and 26 probable double-mode RR Lyrae stars). Other photometric studies were performed by Bellazzini et al. (2002) and Rave et al. (2003).

Draco seems to host a single stellar population older than $\approx 10 \text{ Gyr}$ (Grillmair et al. 1998, Dall'Ora et al. 2003). According to Bonanos et al. (2004), the Draco luminosity ($\approx 2 \times 10^5 L_\odot$) is comparable to that of the faintest luminous systems.

By NED² we get not only the galaxy coordinates but also other interesting quantities such as the mean distance of about 82 kpc and the physical major and minor axes of 1.19 kpc and 0.72 kpc, respectively. McConnachie (2012) reports a position angle of 89° . For our

¹ We mention that the *XMM*-Newton observations analysed in this work (see text for details) have been already used for different purposes. As an example, Malyshev et al. (2014) searched for a 3.55 keV line as the signatures of dark matter (in the form of sterile neutrinos) decays. Their analysis showed no evidence for the presence of such line in the stacked spectra of the investigated dSphs.

² NASA/IPAC Extragalactic Database is available at <http://ned.ipac.caltech.edu>.

study³ we used five *XMM-Newton* observations (IDs 0603190101, 0603190201, 0603190301, 0603190401, and 0603190501) made in the August 2009 for a total exposure time of about 90 ks.

2.2 Leo I

As far as Leo I (at J2000 coordinates $RA = 10^h 08^m 28.1^s$ and $Dec = 12^\circ 18' 23''$) is concerned, NED database gives a mean distance of ≈ 246 kpc (thus it is one of the furthest MW companions), positional angle of 80° , physical major and minor axis of 0.86 kpc and 0.64 kpc, respectively. Harrington & Wilson (1950) analyzed this gas poor galaxy whose type II star population and elliptical shape suggested a similarity with the Sculptor system. The large distance from the MW and the high radial velocity, confirmed by Koch et al. (2007), suggest that Leo I is an isolated dSph, not currently affected by Galactic tidal forces. However, the presence of stars beyond the object tidal radius confirms the hypothesis that some dSphs may be perturbed at least in their outermost regions by the existence of a huge amount of dark matter at large distances.

Recently Smecker-Hane et al. (2009) re-analyzed the star population content of this dwarf galaxy and determined the galaxy star formation rate as a function of time. In particular, they found that Leo I has a stellar population older than previously believed and older than that of the irregular Leo A galaxy, although both systems have continuously formed stars. The evidence of a radial age gradient in the red giant branch (RGB) stellar population was shown by Gullieuszik et al. (2009) who estimated the stellar ages, while Menzies et al. (2010) analyzed the existence of asymptotic giant branch (AGB) variables.

In our work we use the *XMM-Newton* observation (ID 0555870201) of about 90 ks made on 2008-11-24, the same being previously analyzed by Orio et al. (2010). These authors cross-correlated their sample of X-ray detected sources with the catalogue of carbon rich AGB stars in Leo I Held et al. 2010 finding no association. As claimed by Orio et al. (2010), a few X-ray sources correlate in position with RGB stars (most symbiotic binary systems have red giant companions). This is consistent with our results (see Section 3).

2.3 Ursa Major II

UMa II dSph (with J2000 coordinates $RA = 08^h 51^m 30^s$ and $Dec = 63^\circ 07' 48''$) was discovered by Zucker et al. (2006) analyzing Sloan Digital Sky Survey (SDSS). They noted its irregular and distorted shape, probably due to a tidal disruption process. Evidences supporting this scenario are found in morphological studies made by Fellhauer et al. (2007) and Muñoz et al. (2010) to which we

refer for more details. In spite of the dominant dark matter contribution scenario, Smith et al. (2013) demonstrated, via N-Body simulations, that the observed properties can be well reproduced, in absence of DM, by tidal mass loss processes. So the presence/absence of dark matter in UMa II is a not yet settled issue.

Another still open point is related to the star population of this dwarf galaxy. Dall'Ora et al. (2012) revealed hints, although not statistically significant, of two distinct stellar populations, with different age and metallicity. They also detected a RR Lyrae star in UMa II and evaluated a distance of about 34.7 kpc. We use a distance of 34 kpc, as reported by NED, in the analysis of *XMM-Newton* data (ID 0650180201) obtained on 2011-04-21 with an exposure time of about 34 ks. As reported in McConnachie (2012), the galaxy half light radius is $r_h \approx 0.15$ kpc and a position angle of 98° .

2.4 Ursa Minor

The fourth target of our sample is UMi dSph at J2000 coordinates $RA = 15^h 09^m 10.2^s$ and $Dec = 67^\circ 12' 52''$ (Falco et al. 1999).

This dSph is one of the first MW companions revealed in the past century (Wilson 1955). Walker et al. (2007) analyzed the stellar velocity dispersion profiles of some dSphs, among which UMi, observing that it remains approximately constant with the galactocenter distance. The authors also noted that the observed profiles were well fitted by models of luminous stars systems immersed into a DM halo.

Regarding the star formation history, UMi shows a predominantly old (with age of about 10 Gyr) stellar population (Carrera et al. 2002). In that work, the authors studied also the stellar metallicity claiming the absence of a metallicity radial gradient throughout the galaxy. According to NED, UMi has a mean distance of 73 kpc, positional angle of 69° , physical major and minor axis of 0.85 kpc and 0.53 kpc, respectively.

We analyzed two *XMM-Newton* observations (ID 0301690301, and 0301690401) made between the end of August and the beginning of September 2005 for a total exposure time of ≈ 27 ks.

Nucita et al. (2013b) analyzed the X-ray data acquired by the Chandra satellite towards this galaxy and found an X-ray source spatially coincident (within a few arcseconds) with a radio one. Assuming that the target is an accreting IMBH, the authors evaluated the BH mass, which resulted to be $\approx 2.9 \times 10^6 M_\odot$. However, the detection algorithm used did not allow to exclude that one false detection per CCD occurred. Here, to confirm the previous result, here we used *XMM-Newton* observations (see the next Section).

3 XMM-NEWTON DATA REDUCTION AND SOURCE DETECTION

We used the *XMM-Science* Analysis System (SAS version see: <http://xmm.esa.int/sas/>), with the most recent calibration files, to process the observation data files (ODFs).

We obtained the event lists by processing the raw data via the standard *emchain* and *epchain* tools, and following the standard procedures in screening the data provided by the three European Photon Imaging Cameras (MOS 1, MOS 2 and pn) on-board *XMM-Newton* satellite.

We applied the analysis procedure described in Nucita et al. (2013a). Here we only remind that, in accordance with the 2XMM catalogue of serendipitous X-ray sources (Watson et al. 2009), we divided each EPIC camera event list into 5 energy bands, i.e. :

³ For completeness, we note that Draco dSph was observed also by the *Chandra* satellite (IDs 9568 and 9776) with the ACIS-S camera and exposure times of ≈ 24 ks and ≈ 12 ks, respectively. Only four detectors were on during the observations thus limiting the coverage of the Draco galaxy. The event files were reprocessed using the most updated calibration files and the CIAO tool suite (version 4.6). Then, we searched for X-ray sources in the 0.5 – 7 keV by using the *celldetect* code choosing a signal-to-noise ratio of 2.5 for the source detection. After eliminating a few sources not recognized as such by eye, we were left with 9 X-ray targets indicated by yellow diamonds in Figure 1. We remind that the background corrected rates and fluxes of the identified sources are consistent within the errors with those estimated by using *XMM-Newton*.

B_1 : 0.2–0.5 keV, B_2 : 0.5–1.0 keV, B_3 : 1.0–2.0 keV, B_4 : 2.0–4.5 keV, and B_5 : 4.5 – 12.0 keV, producing one image for each energy band, plus a mosaic image in the 0.2–12.0 keV energy band (for inspection purposes only), and carried out the source detection using the SAS task *edetect_chain*.

The exposure map has been evaluated with the *eexmap* task, for each camera and input image, taking into account the calibration information on spatial quantum efficiency, filter transmission and vignetting. Then we produced appropriate image masks to delimit the regions in which to perform source detection with the task *emldetect*. This task applies a point spread function (PSF) fitting algorithm simultaneously in the five energy bands giving as output source coordinates, energy fluxes and hardness ratios (for details see: <http://xmm.esac.esa.int/sas/current/documentation>).

The X-ray fluxes are given in units of $\text{erg s}^{-1} \text{cm}^{-2}$ through the formula

$$F_i = \frac{B_i}{ECF_i}, \quad (1)$$

where the count rate (B_i) and the energy conversion factor (ECF_i) are in units of $10^{11} \text{ counts cm}^2 \text{ erg}^{-1}$ in the i -th band for each EPIC camera. To obtain the latter factors⁴ we assumed a power-law model with photon index $\Gamma = 1.7$ and mean Galactic foreground absorption $N_H \approx 3.0 \times 10^{20} \text{ cm}^{-2}$ (Watson et al. 2009).

Finally, we purged the candidate source lists by requiring a maximum likelihood threshold equal to 10, corresponding to 4σ , and removing a few spurious sources identified as false detections or positioned at the borders of the cameras. Our results are consistent with the 3XMMi-DR4 with minor differences due to the fact that we have excluded few spurious sources.

At the end of the procedure, we obtained 89, 116, 49 and 54 sources for Draco, Leo I, UMa II and UMi, respectively. Previously, Orío et al. (2010) analyzed the same Leo I data set detecting 105 X-ray sources. We impute the discrepancy to slightly different choices in the data screening procedure and the detection threshold used.

The logarithmically scaled 0.2–12 keV images (smoothed with a 3 pixel gaussian kernel) are shown in Fig. 1. For Draco, Leo I and UMi the dashed circles represent the extension of the galaxies as suggested by the NASA/IPAC extragalactic database, while in the case of UMa II we used the half light radius taken from McConnachie (2012). In each panel, the $35''$ radius circles containing $\approx 90\%$ of energy at 1.5 keV in the pn camera (see e.g., de La Calle et al. 2014) indicate the detected sources each of which is labeled with a sequential number following the 0.2–12.0 keV increasing flux order.

In Tables 1 - 4 we report the main results of our analysis, showing the detected sources in increasing flux order. For each source, the first two columns show, respectively an identification number and a label (#) indicating how many times it was revealed in the XMM-Newton observations, i.e.: A - once, B - twice, C - three times, and so on. In Leo I and UMa II cases there are only A sources because we used a single observation. Columns 3–5 report the J2000 coordinates with the associated errors. Column 6 reports the 0.2–12.0 keV absorbed flux. To get the parameter $\log(f_X/f_{opt})$

(column 7), the SIMBAD⁵ archive was searched for correlations (within a radius of $3''$) from which we extracted the relevant magnitude in the V band or, if not available, the average between R and B ones (Bartlett et al. 2012). The high-energy hardness-ratios HR_1^* , HR_2^* and HR_i with $i = 1, \dots, 4$ (see next section) are shown in the remaining columns. In Tables 5 - 8 we present the correlation with catalogued counterparts, if any. For this purpose, we used several databases to correlate our X-ray source catalogue with optical counterparts, namely: the Two Micron All-Sky Survey (2MASS), the Two Micron All-Sky Survey Extended objects (2MASX, Skrutskie et al. 2006), the United States Naval Observatory all-sky survey (USNO-B1, Monet et al. 2003), the position and proper motions extended catalogues (PPMX, Roeser et al. 2008 and PPMXL, Roeser et al. 2010), the QSO candidates in the SDSS stripes examined (J/MNRAS/396/223/qsos, D'Abrusco et al. 2009), the candidate AGN objects catalogue (J/MNRAS/437/968, Cavuoti et al. 2014). Regarding Draco dSph, we also searched for long-period, semi-regular red variable stars, carbon stars and eclipsing binaries (J/AJ/136/1921/table9, Kinemuchi et al. 2008), QSOs found in the same survey (J/AJ/136/1921/table10, Kinemuchi et al. 2008), variable stars (J/AJ/127/861, Bonanos et al. 2004), and late-type stars (J/A+A/442/165, Cioni & Habing 2005). The quasar-galaxy associations catalogue (J/AZh/78/675, Bukhmastova 2001) was used for the analysis of both Draco and UMi.

In the Leo I case, we used the NIR catalogue obtained with the WFCAM wide-field array at the United Kingdom Infrared Telescope (J/MNRAS/404/1475/table2, Held et al. 2010), while the Palomar Transient Factory (PTF) photometric catalogue 1.0 (II/313, Ofek et al. 2012) was compared with UMa II source list. Moreover, for UMi dSph we examined the catalogue of quasar candidates from non-parametric Bayes classifier kernel density estimate (JApJS/180/67, Richards et al. 2010) and the atlas of Radio/X-ray associations (V/134/arxa, Flesch 2010).

For details about the limiting magnitude of the used catalogues we remind to the relevant publications. Here, for example, we remind that 2MASS has limiting sensitivity of 17.1, 16.4 and 15.3 mag in J, H, and K bands, respectively, while the USNO-B1 catalogue is complete down to a visual magnitude of ≈ 21 and has positional accuracy of $\approx 0.2''$. Note that some catalogues (as PPMX and PPMXL, or 223/qsos and 437/968) refer to other well known catalogues (as 2MASS and USNO-B1, or SDSS) and inherit the corresponding limiting magnitudes.

Therefore, we associated to the coordinates of each of the identified X-ray sources an error resulting from the quadrature sum of the XMM-Newton positional accuracy ($\approx 2''$ at 2σ confidence level, see Kirsch 2004 and Guainazzi 2010) and the statistical error as determined by the *edetect_chain* tool. Since the resulting positional uncertainty is of the order of a few arcseconds, we do not over-plot the source error circles in any figure of this paper. In the same way, the error associated with the optical counterpart was derived from the relevant catalogues.

Only if an X-ray source is found to be within 1σ (and 3 arcsec) from a catalogue counterpart, we report the corresponding distance in arcseconds in Tables 5 - 8. In the case of multiple sources satisfying the previous condition, the source having the minimum distance from the X-ray target was used. We also show the object type (OType) category of the counterpart, as reported in the SIMBAD archive⁶, as well as our own source classification (HR Class).

⁴ For ECFs and associated correction factors, see the User's Guide of the 2XMM catalogue of serendipitous sources available at

<http://xmssc-www.star.le.ac.uk/Catalogue/2XMMi-DR3>. We note that our results are consistent within a few percent when relaxing the adopted assumptions.

⁵ <http://simbad.u-strasbg.fr/simbad/>

⁶ The SIMBAD object classification (class standard designation,

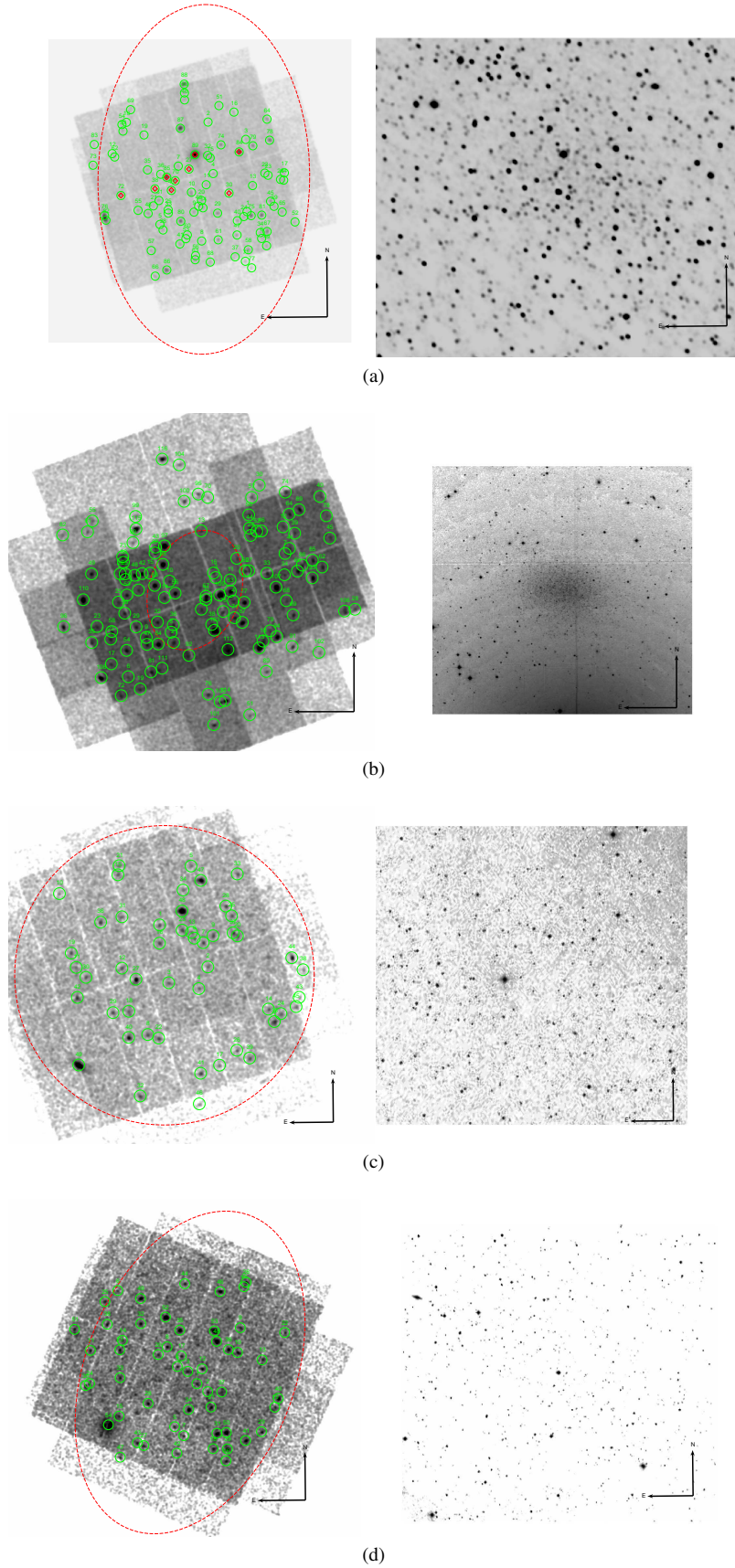


Figure 1. Mosaic images of the XMM-Newton MOS 1, MOS 2, and pn exposures in the 0.2-12.0 keV energy band of the sample galaxies.

A XMM-Newton observation of a sample of four close dSph galaxies. 7

Table 1: The X-ray sources towards the Draco dSph as detected by the XMM-Newton satellite. The full list is available on-line.

Src	#	RA (J2000)	DEC (J2000)	ERR arcsec	$F_{0.2-12keV}^{Abs}$ $\times 10^{-14} \text{ erg s}^{-1} \text{ cm}^{-2}$	$\log\left(\frac{f_X}{f_{opt}}\right)$	HR_1^*	HR_2^*	HR_1	HR_2	HR_3	HR_4
1	A	17 19 26.1	57 50 18.7	2.546	≤ 1.21		0.08 ± 0.58	-0.66 ± 0.67	0.71 ± 0.22	-0.83 ± 0.20	-1.00 ± 1.01	1.00 ± 0.64
2	A	17 20 07.8	58 03 5.8	2.558	≤ 1.09	0.131	-0.07 ± 0.64	-0.26 ± 0.68	0.01 ± 0.30	0.29 ± 0.30	-1.00 ± 0.22	1.00 ± 0.23
3	A	17 19 27.2	58 00 36.3	2.418	0.54 ± 0.45	-1.314	0.28 ± 0.55	-0.44 ± 0.56	-0.11 ± 0.29	-0.35 ± 0.29	-0.76 ± 0.47	1.00 ± 0.14
4	C	17 20 02.3	57 55 44.5	2.510	0.55 ± 0.27		-0.08 ± 0.63	-0.13 ± 0.69	0.18 ± 0.25	0.01 ± 0.25	-0.24 ± 0.31	-0.64 ± 0.37
5	A	17 20 59.4	57 48 28.7	2.567	≤ 1.29		-0.22 ± 0.73	-0.09 ± 0.64	-0.04 ± 0.20	0.27 ± 0.24	-0.46 ± 0.27	-0.94 ± 0.94
6	A	17 19 10.6	57 46 28.3	2.591	≤ 1.31		-0.13 ± 0.79	-0.02 ± 0.59	0.37 ± 0.31	0.28 ± 0.25	-0.42 ± 0.26	-1.00 ± 0.93
7	A	17 20 39.8	57 56 48.2	2.427	0.66 ± 0.37		0.09 ± 0.65	0.23 ± 0.56	-0.10 ± 0.31	0.68 ± 0.21	-0.13 ± 0.25	-0.23 ± 0.31
8	A	17 20 14.7	57 46 07.5	2.578	0.70 ± 0.62		-0.14 ± 0.68	0.14 ± 0.59	0.35 ± 0.31	0.28 ± 0.22	-0.20 ± 0.23	-1.00 ± 0.48
9	B	17 20 22.9	57 50 14.8	3.287	0.71 ± 0.33		0.00 ± 0.63	0.20 ± 0.57	0.67 ± 0.44	0.53 ± 0.23	0.01 ± 0.21	-0.75 ± 0.21

Table 2: The X-ray sources towards the LeoI dSph as detected by the XMM-Newton satellite. The full list is available on-line.

Src	#	RA (J2000)	DEC (J2000)	ERR arcsec	$F_{0.2-12keV}^{Abs}$ $\times 10^{-14} \text{ erg s}^{-1} \text{ cm}^{-2}$	$\log\left(\frac{f_X}{f_{opt}}\right)$	HR_1^*	HR_2^*	HR_1	HR_2	HR_3	HR_4
1	A	10 08 56.2	12 19 27.2	2.480	0.15 ± 0.14		-0.16 ± 0.60	-0.01 ± 0.49	0.27 ± 0.26	0.09 ± 0.22	-0.76 ± 0.24	0.42 ± 0.38
2	A	10 08 50.9	12 18 24.8	2.403	0.20 ± 0.15		-0.39 ± 0.54	-0.03 ± 0.49	0.20 ± 0.22	0.22 ± 0.17	-0.95 ± 0.14	0.76 ± 1.14
3	A	10 08 19.5	12 19 38.6	2.344	0.21 ± 0.13	-0.870	-0.12 ± 0.59	-0.17 ± 0.57	-0.03 ± 0.22	-0.03 ± 0.24	-0.40 ± 0.33	0.06 ± 0.51
4	A	10 08 12.4	12 17 18.7	2.358	0.21 ± 0.14		-0.32 ± 0.53	0.04 ± 0.46	0.63 ± 0.17	-0.08 ± 0.16	-0.35 ± 0.21	-0.99 ± 0.71
5	A	10 08 25.4	12 16 29.9	2.358	0.22 ± 0.11		-0.15 ± 0.37	-0.53 ± 0.46	0.27 ± 0.16	-0.44 ± 0.18	-0.86 ± 0.35	0.34 ± 0.85
6	A	10 08 55.0	12 09 47.9	2.475	≤ 0.50		-0.06 ± 0.77	-0.52 ± 0.77	-0.22 ± 0.20	-0.19 ± 0.26	-0.22 ± 0.40	-1.00 ± 1.39
7	A	10 07 51.4	12 22 01.9	2.408	≤ 0.58		0.08 ± 0.77	0.02 ± 0.54	-0.98 ± 0.12	0.98 ± 0.16	-0.20 ± 0.30	0.09 ± 0.34
8	A	10 08 37.6	12 14 13.2	2.350	0.26 ± 0.17		-0.18 ± 0.52	-0.05 ± 0.45	0.26 ± 0.22	0.11 ± 0.20	-0.47 ± 0.24	0.33 ± 0.51
9	A	10 08 47.8	12 13 41.6	2.651	0.30 ± 0.12		-0.14 ± 0.38	-0.08 ± 0.36	0.49 ± 0.18	0.06 ± 0.15	-0.28 ± 0.18	-0.99 ± 0.40
10	A	10 08 38.3	12 19 17.1	2.321	0.33 ± 0.15		-0.21 ± 0.52	-0.12 ± 0.46	-0.09 ± 0.17	0.32 ± 0.19	-0.94 ± 0.16	0.81 ± 0.50

Table 3: The X-ray sources towards the UMaII dSph as detected by the XMM-Newton satellite. The full list is available on-line.

Src	#	RA (J2000)	DEC (J2000)	ERR arcsec	$F_{0.2-12keV}^{Abs}$ $\times 10^{-14} \text{ erg s}^{-1} \text{ cm}^{-2}$	$\log\left(\frac{f_X}{f_{opt}}\right)$	HR_1^*	HR_2^*	HR_1	HR_2	HR_3	HR_4
1	A	08 51 34.3	63 12 48.2	2.414	0.67 ± 0.48		-0.24 ± 0.41	-0.45 ± 0.50	0.58 ± 0.17	-0.38 ± 0.17	-0.90 ± 0.23	-1.00 ± 2.82
2	A	08 50 51.9	63 08 37.6	2.578	0.68 ± 0.25		-0.08 ± 0.65	0.30 ± 0.65	0.15 ± 0.42	0.64 ± 0.23	-0.16 ± 0.23	-1.00 ± 0.19
3	A	08 51 26.3	63 07 03.7	2.431	0.69 ± 0.32		-0.08 ± 0.52	-0.08 ± 0.55	0.56 ± 0.27	0.28 ± 0.22	-0.32 ± 0.22	-0.38 ± 0.35
4	A	08 50 59.9	63 06 28.6	2.496	0.80 ± 0.48		-0.23 ± 0.71	0.22 ± 0.63	0.25 ± 0.39	0.54 ± 0.24	-0.47 ± 0.22	-0.93 ± 0.49
5	A	08 51 06.5	63 18 38.9	2.708	0.83 ± 0.56		-0.31 ± 0.51	-0.24 ± 0.59	0.67 ± 0.19	-0.17 ± 0.22	-0.90 ± 0.15	-1.00 ± 0.73
6	A	08 51 03.7	63 11 29.1	2.449	0.87 ± 0.32		-0.30 ± 0.57	0.06 ± 0.56	0.53 ± 0.28	0.15 ± 0.20	-0.41 ± 0.24	-0.89 ± 0.30
7	A	08 50 55.9	63 11 02.2	2.246	1.01 ± 0.37		-0.21 ± 0.32	-0.44 ± 0.41	0.48 ± 0.14	-0.44 ± 0.15	-0.85 ± 0.25	-0.29 ± 0.82
8	A	08 51 44.6	63 01 55.2	2.303	1.18 ± 0.51		-0.29 ± 0.39	-0.19 ± 0.45	0.43 ± 0.17	-0.04 ± 0.17	-0.81 ± 0.17	0.62 ± 0.45
9	A	08 50 47.3	63 11 43.6	2.323	1.20 ± 0.50		-0.21 ± 0.41	-0.08 ± 0.43	0.14 ± 0.23	0.34 ± 0.16	-0.66 ± 0.16	-0.49 ± 0.46
10	A	08 53 02.7	63 15 53.0	2.505	≤ 3.14		-0.10 ± 0.50	-0.46 ± 0.59	0.51 ± 0.27	-0.21 ± 0.27	-0.70 ± 0.27	-1.00 ± 0.92

Table 4: The X-ray sources towards the UMi dSph as detected by the XMM-Newton satellite. The full list is available on-line.

Src	#	RA (J2000)	DEC (J2000)	ERR arcsec	$F_{0.2-12keV}^{Abs}$ $\times 10^{-14} \text{ erg s}^{-1} \text{ cm}^{-2}$	$\log\left(\frac{f_X}{f_{opt}}\right)$	HR_1^*	HR_2^*	HR_1	HR_2	HR_3	HR_4
1	A	15 09 01.8	67 11 31.9	2.582	0.59 ± 0.34	-0.923	-0.32 ± 0.66	0.16 ± 0.70	-0.20 ± 0.35	0.38 ± 0.28	-0.38 ± 0.24	-1.00 ± 0.31
2	A	15 08 48.6	67 10 34.6	2.708	0.72 ± 0.59		-0.34 ± 0.79	0.20 ± 0.83	0.17 ± 0.44	0.37 ± 0.28	-0.28 ± 0.23	-0.66 ± 0.40
3	A	15 09 13.1	67 12 59.4	3.052	0.73 ± 0.29		-0.18 ± 0.52	-0.33 ± 0.67	0.42 ± 0.24	-0.33 ± 0.24	-0.66 ± 0.19	-1.00 ± 0.29
4	A	15 09 25.9	67 13 35.3	2.477	0.85 ± 0.45		-0.25 ± 0.73	0.27 ± 0.71	0.71 ± 0.23	0.37 ± 0.26	-0.51 ± 0.24	-0.17 ± 0.38
5	A	15 09 29.2	67 06 24.6	2.779	0.88 ± 0.64	-0.402	-0.19 ± 0.45	-0.23 ± 0.54	0.24 ± 0.31	-0.01 ± 0.28	-0.39 ± 0.32	-1.00 ± 1.03
6	A	15 10 39.6	67 22 36.6	2.912	≤ 3.59	0.717	-0.01 ± 0.98	-0.49 ± 0.96	-0.01 ± 0.29	-0.32 ± 0.39	-0.09 ± 0.90	-1.00 ± 2.72
7	A	15 09 18.0	67 05 20.3	2.607	0.98 ± 0.67		-0.06 ± 0.33	-0.67 ± 0.45	0.51 ± 0.22	-0.74 ± 0.17	-0.29 ± 0.58	-1.00 ± 1.63
8	A	15 09 38.4	67 15 56.0	2.414	1.12 ± 0.51	0.507	-0.42 ± 0.58	0.28 ± 0.56	-0.01 ± 0.24	0.61 ± 0.15	-0.76 ± 0.18	-0.49 ± 0.47
9	A	15 08 08.1	67 18 10.8	2.573	1.17 ± 0.89	0.478	-0.14 ± 0.55	-0.39 ± 0.63	0.11 ± 0.24	-0.01 ± 0.25	-0.78 ± 0.26	0.62 ± 0.53
10	A	15 08 11.7	67 15 14.4	2.339	1.24 ± 0.82	0.407	-0.19 ± 0.47	-0.26 ± 0.49	0.13 ± 0.20	-0.04 ± 0.20	-0.36 ± 0.23	-1.00 ± 0.82

4 HIGH-ENERGY VIEW

In the following section we address the problem of the membership of our X-ray sources to the dSph galaxies, mainly through the analysis of high-energy data.

4.1 Hardness-Ratios and X-ray-to-NIR Flux Diagrams

With the aim to attempt a classification of the high-energy sources detected towards our dSph sample, we followed Ramsay & Wu (2006) and calculated the hardness-ratios (HR^*) as

$$HR_1^* = \frac{H - M}{S + M + H} \quad \text{and} \quad HR_2^* = \frac{M - S}{S + M + H}. \quad (2)$$

Here, S, M, and H correspond to the count rates in the 0.2-1.0 keV, 1.0-2.0 keV, and 2.0-12.0 keV energy bands. From these HR^* values we constructed the color-color diagrams shown in Fig. 2, where the obtained values are compared with two spectral models. We used bremsstrahlung (grey tracks) and power-law (black lines) models in order to simulate the HR_1^* and HR_2^* of Cataclysmic Variables (CVs), Active Galactic Nuclei (AGN) or X-ray binaries⁷, respectively.

We used the XSPEC package (Arnaud 1996) version 12.0.0 to obtain the color-color contours. In both cases, we vary the equivalent hydrogen column density N_H from 10^{19} cm^{-2} to 10^{22} cm^{-2} so each of the almost horizontal lines corresponds to models with equal N_H which increases from bottom to top. The temperature associated to each bremsstrahlung model (kT, taken in the range 0.1 - 3.0 keV) and the power-law index Γ (in the range 0.1 - 3.0) are associated with primarily vertical lines: the values of kT and Γ increase from left to right and from right to left, respectively.

In the upper left side of each panel of Fig. 2 we give a representative error bar, obtained by averaging all the data point error bars. Some of the detected sources have colors consistent with those of the absorbed power-law or absorbed bremsstrahlung models, others seem to require combined spectra or fall outside the pattern area. Even if many sources appear to have spectra consistent with that of a typical AGN (squared dots close black tracks) we cannot rule out that some of the sources have a different nature. In fact, due to the large error bars affecting HR^* values, a classification based only on the hardness-ratio cannot constrain the nature of the objects in our sample, allowing to distinguish among AGNs, X-ray binaries, CVs and X-ray active stars.

In order to improve our classification, we adopted the method of Haakonsen & Rutledge (2009) that uses a color-color diagram based on the ratio between the 0.2 - 2.4 keV flux (F_X) and the NIR flux in the J band (F_J) versus the J-K color. In particular, QSO and Seyfert 1 objects lie in the upper right part having $(J - K) \gtrsim 0.6$ and $F_X/F_J \gtrsim 3 \times 10^{-2}$ (dashed red lines in Fig. 3) and the coronally active stars (including pre-main sequence and main-sequence stars, high proper-motion objects and binary systems) the lower left side with $(J - K) \lesssim 1.1$ (dotted black line in Fig. 3) and $F_X/F_J \lesssim 3 \times 10^{-2}$.

As one can see in Tables 1 - 4 we found many correlations between the detected sources and 2MASS catalogue. For these sources, we give in Tables 9 the 0.2-2.4 keV and NIR J band fluxes, as well as the J and K magnitudes. To obtain the 0.2-2.4 keV band flux we used the 0.2-12.0 keV one assuming, in webPIMMS⁸, a

power-law model with spectral index Γ and absorption column density N_H inferred by NASA on-line tool⁹. Thus we obtained $\Gamma=1.7$ and $N_H=2.77 \times 10^{20} \text{ cm}^{-2}$ for Draco, $\Gamma=1.7$ and $N_H=3.75 \times 10^{20} \text{ cm}^{-2}$ for Leo I, $\Gamma=1.7$ and $N_H=4.65 \times 10^{20} \text{ cm}^{-2}$ for UMa II and $\Gamma=1.7$ and $N_H=2.20 \times 10^{20} \text{ cm}^{-2}$ for UMi. In Fig. 3, we present the color-color diagrams for the sources listed in Table 9.

In particular, Fig. 3 (a) shows the fifteen sources of Draco dSph with the detected counterparts. Among these, three (55, 80 and 88) clearly reside in the AGN part of the diagram. The likely galactic nature of source 55 is also inferred by the correlation with a QSO (see catalogues 223/qsos and 1921/table10). Instead sources 1, 3, 10, 14, 19, 29, 38, 42, 87, and 89 can be stellar objects. Many of them (1, 10, 19, 38, 87, 89) correlate with PPMX sources so are probably Milky Way sources. Src 38 is also associated with an object belonging to a late-type stars catalogue (442/165), while Src 29 is realistically a “carbon star (C1)”, as also reported in the Draco stellar catalogue 1921/table9. Src 10 may be either a star (PPMX catalogue) or a background (437/968) object. In this case, the use of the diagram can be useful to settle the querelle in favour of a stellar type. We cannot use the same method for Src 13, correlating with both PPMX (stellar) and 78/675 (quasar-galaxy association) catalogues, because of its not clear identification in the aforementioned regions of the diagram. Finally, Src 39 is not catalogued with our diagram although it seems correlated with an AGN candidate (437/968 catalogue).

In the Leo I case we find four sources correlating with the 2MASS catalogue. The position of Src 113 in Fig. 3 (b) denotes its background nature. The sources 96 and 108, recognized as stellar sources, are also associated with two objects in the PPMX catalogue, so they can be foreground stars.

Fig. 3 (c) shows five (1, 7, 8, 27, 44) stellar and three (21, 48, 49) galactic sources toward UMa II dSph. We correctly obtain a correlation of Src 27 with a source in the PPMX catalogue. In the same catalogue we find a source correlating with Src 44 that has an association with an AGN candidate (437/968 catalogue) so the diagram is useful in order to fix the possible stellar nature of the source.

In the last panel of Fig. 3, named (d), we present the analysis for UMi dSph. The relevant sources (1, 13 and 47) seem to have characteristics similar to X-ray active stars and binary sources. In particular, Src 13 correlates with a Radio/X-ray source (V/134 catalogue) with Red [Blue] magnitude of 17.0 [20.2] while Src 47, correlating also with PPMX catalogue, is probably a foreground star.

We also used the SIMBAD database to search for correlations between our X-ray sources and available catalogues, getting more information (e.g., magnitude, redshift, source interpretation) afterwards used.

Moreover we follow the method of Pietsch et al. (2004), already used by Bartlett et al. (2012) to classify high-energy sources in Phoenix dSph. These authors statistically evaluated the nature of the sources by considering some criteria based on HR values defined as $HR_i = (B_{i+1} - B_i)/(B_{i+1} + B_i)$, with the count rates B_i of the bands already given in S 3. We get our own criteria, summarized in Table 10, using the criteria fixed by Bartlett et al. (2012) and requesting the relevant classification in SIMBAD (for results of our classification, see Fig. 4 and Table 11). The sources are labelled

⁷ The reader can also see Ramsay & Wu (2006).

⁸ WebPIMMS is available at

<http://heasarc.gsfc.nasa.gov/Tools/w3pimms.html>

⁹ This tool is available at

<http://heasarc.gsfc.nasa.gov/cgi-bin/Tools/w3nh/w3nh.pl>

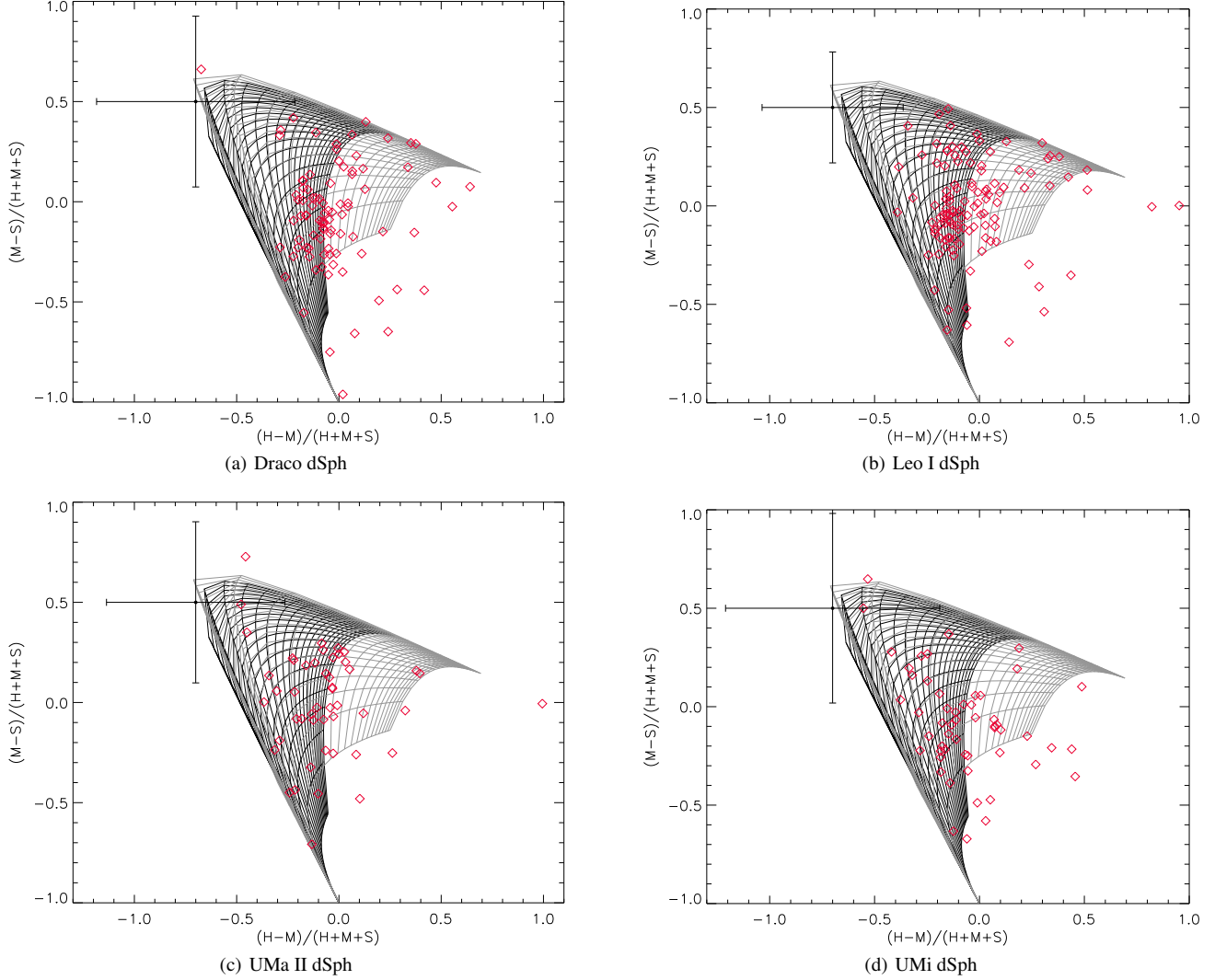


Figure 2. The color-color diagram of the sources detected by the EPIC cameras towards the dSphs. The solid lines represent the theoretical tracks expected for different emitting models (see text for details). A representative error bar (obtained averaging all data point error bars) is also shown in each panel.

identified (i), classified (cl) or candidate (ca) if they fulfill all, the majority or only few criteria, respectively.

Furthermore, in the last column of Tables 5-8 we report the source classification (HR Class.) based on these criteria. Here, FG [fg/f] point out the identified [classified/candidate] foreground stars, snr the classified Super Nova Remnants, A the identified Active Galactic Nuclei, G [g] the identified [classified] galaxies, sss the classified super soft sources, h the classified hard sources and Loc [loc/l] the identified [classified/candidate] local X-ray sources.

As the reader can see, the obtained results allow to get a wider X-ray source classification and show a good agreement with the previous inferences.

4.2 Background sources

As suggested in the previous discussion, some of the detected sources may be AGNs or background galaxies. We estimate the expected number of background sources towards our targets through the logN-logS diagram (Hasinger et al. 2005). Starting from the minimum absorbed fluxes (in the 0.2-12.0 keV energy band) and assuming Γ and N_H values as in the previous section, we estimated,

via webPIMMS v3.9, the unabsorbed fluxes in the 0.5-2.0 keV energy band to be

$$F_{0.5-2.0}^{Unabs} = 1.67 \times 10^{-15} \text{ erg s}^{-1} \text{ cm}^{-2} \text{ for Draco,}$$

$$F_{0.5-2.0}^{Unabs} = 4.73 \times 10^{-16} \text{ erg s}^{-1} \text{ cm}^{-2} \text{ for Leo I,}$$

$$F_{0.5-2.0}^{Unabs} = 2.15 \times 10^{-15} \text{ erg s}^{-1} \text{ cm}^{-2} \text{ for UMa II,}$$

$$F_{0.5-2.0}^{Unabs} = 1.80 \times 10^{-15} \text{ erg s}^{-1} \text{ cm}^{-2} \text{ for UMi.}$$

Using these values as input parameters in the Hasinger relation, we find the expected number of background AGNs as a function of the angular distance from the galaxy center. In order to compare the theoretically estimated source number with the observed one, we divided each dSph field of view (FOV) into five rings and performed therein the comparison. As it can be seen in Table 12, the number of X-ray sources in each annulus is generally consistent with the expected one, although this is not the case for the external annuli since the logN-logS does not account for border effects.

Nevertheless, we cannot rule out that some sources actually belong to MW or to the dSphs. This claim is supported by the presence of X-ray sources in the bottom-left region of the panels in Fig. 3 and the correlations with variable stars catalogues and the analysis summarized in the following section as well.

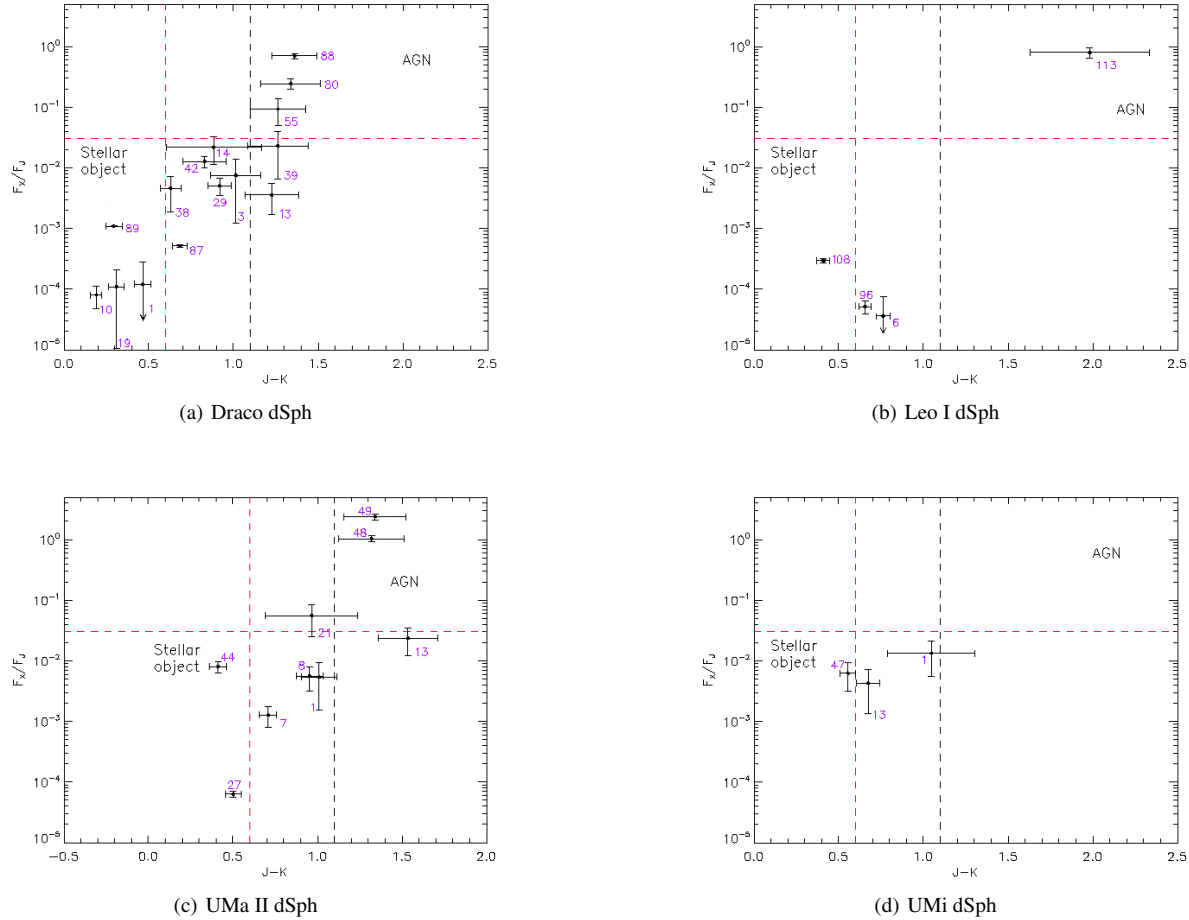


Figure 3. The color-color diagram for our X-ray sources with a counterpart in the 2MASS catalogue (see text for details).

4.3 Possible local stars

As next we investigate the local nature of some of the detected high-energy sources.

Draco sources 3, 14 and 42, recognized as stellar objects in Fig. 3 (a), are not associated with any of the sources in the PPMX catalogue and so it cannot be excluded that they are local high-energy stellar systems. Src 30 has a “carbon like star counterpart” at a distance of $0.38''$, as reported by the 1921/table9 catalogue that collects many kinds of stars belonging to Draco. Sources 60, 64 and 77 correlate with late-type stars in Draco but Src 64 and 77 have closer counterparts in two background object catalogues as well. Finally, Src 84 is associated with a Draco variable star (within $1''$) of the 127/861 catalogue but also to a QSO at distance of $0.52''$ [$0.55''$] in the 1921/table10 [1223/qsos] catalogue. Its local nature is not so clear and we must conclude that Src 84 is likely linked to a background source, owing to the smaller distance from this kind of counterpart. The background nature of the last three sources is confirmed by the SIMBAD database. In the same data collection we find clues for stellar nature of X-ray sources toward/in Draco dSph.

As regards Leo I dSph, we find twenty correlations between our catalogue and 1475/table2 one, a NIR catalogue of Leo I stars. One of these sources (Src 103) also correlates (within $\approx 2.27''$) with a QSO candidate, so we infer a possible background nature

for it. Instead Src 6 seems to have a stellar nature (as already seen in Sect. 4.1) and no association with PPMX sources, therefore we argue that it belongs to Leo I galaxy.

In the UMa II case, sources 1, 7 and 8 may belong to this dSph because of their stellar nature (see the aforementioned Sect. 4.1) and no association with any PPMX object. Furthermore sources 7 and 8 correlate with objects in II/313 catalogue, a list of not variable sources. According to their “stellarity index”, a star/galaxy discriminator defined by Ofek et al. (2012), these two sources seem not to have an extended profile and could be UMa II stars, lacking foreground hints.

As for UMi, sources 1 and 13 are probably stars that belong to UMi because they are recognized as likely stellar objects in Fig. 3 (d) but don’t show any correlations with the PPMX catalogue.

We also perform a more restrictive source analysis, using the method deduced from Pietsch et al. (2004) and Bartlett et al. (2012) and considering as local sources only those identified or classified as such. Therefore, in the Draco dSph case we have two local sources (the identified 29 and the classified 14), only one (the classified 14) for UMa II and none as for Leo I and UMi. A subsequent follow-up (also in other wavelengths) would be useful to fully probe the nature of such objects. In addition, it could have some implications in the formation and evolution scenarios of these galactic systems.

(a) Draco dSph				
Src	F_X ($\times 10^{-14}$ erg s $^{-1}$ cm $^{-2}$)	F_J ($\times 10^{-13}$ erg s $^{-1}$ cm $^{-2}$)	J	K
1	≤ 0.48	173.6 ± 3.7	11.17 ± 0.02	10.70 ± 0.02
3	0.21 ± 0.18	2.87 ± 0.19	15.62 ± 0.07	14.61 ± 0.08
10	0.28 ± 0.12	351.6 ± 5.5	10.40 ± 0.02	10.21 ± 0.02
13	0.33 ± 0.17	9.11 ± 0.69	14.37 ± 0.08	13.14 ± 0.08
14	0.33 ± 0.16	1.52 ± 0.15	16.31 ± 0.10	15.42 ± 0.18
19	0.37 ± 0.34	343.3 ± 8.2	10.43 ± 0.03	10.12 ± 0.02
29	0.45 ± 0.14	8.97 ± 0.26	14.38 ± 0.03	13.46 ± 0.04
38	0.61 ± 0.36	13.29 ± 0.38	13.96 ± 0.03	13.33 ± 0.03
39	0.61 ± 0.44	2.67 ± 0.20	15.70 ± 0.08	14.44 ± 0.10
42	0.68 ± 0.14	5.32 ± 0.24	14.95 ± 0.05	14.12 ± 0.08
55	1.04 ± 0.46	1.12 ± 0.17	16.64 ± 0.16	15.38 ± 0.02
80	5.19 ± 0.86	2.13 ± 0.18	15.94 ± 0.09	14.60 ± 0.09
87	10.70 ± 0.56	2086 ± 37	8.47 ± 0.02	7.78 ± 0.02
88	28.9 ± 2.3	4.14 ± 0.24	15.22 ± 0.06	13.86 ± 0.07
89	44.48 ± 0.55	4090 ± 115	7.74 ± 0.03	7.44 ± 0.02
(b) Leo I dSph				
Src	F_X ($\times 10^{-14}$ erg s $^{-1}$ cm $^{-2}$)	F_J ($\times 10^{-13}$ erg s $^{-1}$ cm $^{-2}$)	J	K
6	≤ 0.20	262 ± 5	10.72 ± 0.02	9.96 ± 0.02
96	1.90 ± 0.46	3716 ± 62	7.84 ± 0.02	7.18 ± 0.02
108	3.29 ± 0.27	1117 ± 22	9.15 ± 0.02	8.74 ± 0.02
113	5.70 ± 0.45	0.71 ± 0.15	17.14 ± 0.21	15.16 ± 0.15
(c) UMa II dSph				
Src	F_X ($\times 10^{-14}$ erg s $^{-1}$ cm $^{-2}$)	F_J ($\times 10^{-13}$ erg s $^{-1}$ cm $^{-2}$)	J	K
1	0.27 ± 0.19	4.94 ± 0.23	15.03 ± 0.05	14.02 ± 0.06
7	0.40 ± 0.15	31.54 ± 0.78	13.02 ± 0.03	12.31 ± 0.03
8	0.47 ± 0.20	8.36 ± 0.27	14.46 ± 0.04	13.51 ± 0.04
13	0.64 ± 0.30	2.70 ± 0.13	15.69 ± 0.09	14.15 ± 0.08
21	0.92 ± 0.49	1.66 ± 0.16	16.22 ± 0.10	15.25 ± 0.17
26	1.23 ± 0.59	0.83 ± 0.12	16.96 ± 0.15	–
27	1.24 ± 0.14	1973 ± 42	8.53 ± 0.02	8.03 ± 0.02
44	3.92 ± 0.77	49.2 ± 1.2	12.54 ± 0.03	12.13 ± 0.02
48	22.1 ± 1.3	2.14 ± 0.20	15.94 ± 0.10	14.62 ± 0.10
49	63.7 ± 4.8	2.67 ± 0.23	15.70 ± 0.09	14.36 ± 0.09
(d) UMi dSph				
Src	F_X ($\times 10^{-14}$ erg s $^{-1}$ cm $^{-2}$)	F_J ($\times 10^{-13}$ erg s $^{-1}$ cm $^{-2}$)	J	K
1	0.23 ± 0.14	1.75 ± 0.15	16.16 ± 0.09	15.11 ± 0.17
13	0.52 ± 0.36	12.26 ± 0.30	14.04 ± 0.03	13.37 ± 0.04
47	2.4 ± 1.2	37.47 ± 0.76	12.83 ± 0.02	12.28 ± 0.02

Table 9. The detected X-ray sources that correlate with the 2MASS catalog. Following Haakonsen & Rutledge (2009), we try to constrain their nature by using the X-ray (in the 0.2-2.4 keV band) and NIR (J and K bands) fluxes (see text and Fig. 3 for details). We remind that the 2MASS data reach the 3σ limiting sensitivity of 17.1, and 15.3 mag in the J and K bands, respectively. A long dash means that the corresponding source was not detected in the relevant band.

Apart from the aforementioned sources, about thirty of them remain at the candidate stage. So, a further study could settle the issue if they really belong to the dSphs or not.

4.4 Clues for IMBHs

Both the $M_{BH}-\sigma$ and $M_{BH}-M_{Bulge}$ relations (e.g., Gebhardt et al. 2000 and Ferrarese & Merrit 2000) suggest to search for compact objects, belonging to IMBH's range, toward dSphs. For this reason we investigate the presence of BHs in their cores, where these

Src Type	Criteria
fg star	classified as star in SIMBAD, $\log\left(\frac{f_X}{f_{opt}}\right) < -1.0$ and $HR_2 < 0.3$ and $HR_3 < -0.4$ or not defined
SNR	classified as SNR in SIMBAD, $HR_1 > 0.1$ and $HR_2 < -0.4$ and not a fg star
AGN	classified as AGN, Sy1 or QSO in SIMBAD, not classification as SNR from HR_2
GAL	classified as G in SIMBAD, Optical id with galaxy and $HR_2 < 0.0$
SSS	$HR_1 < -0.2$, $HR_2 - EHR_2 < -0.99$ or HR_2 not defined, HR_3 and HR_4 not defined
HARD	$HR_2 - EHR_2 > -0.2$ or only HR_3 and HR_4 defined and no other classification
LX	not a fg star, classified as star in SIMBAD, redshift compatible with dSph's one

Table 10. Our source classification criteria. Here LX stands for "Local X-ray source".

Type	Draco	Leo I	UMa II	UMi
fg star	$5^i + 7^{cl} + 13^{ca}$	$2^i + 24^{ca}$	11^{ca}	$1^i + 8^{cl} + 8^{ca}$
SNR	1^{cl}	2^{cl}	0	4^{cl}
AGN	11^i	1^i	1^i	2^i
GAL	1^{cl}	$1^i + 1^{cl}$	0	0
SSS	0	0	0	0
HARD	28^{cl}	72^{cl}	31^{cl}	10^{cl}
LX	$1^i + 1^{cl} + 13^{ca}$	1^{ca}	1^{cl}	16^{ca}
not class	8	12	5	5

Table 11. Results of dSphs sources classification made using Table 10 (see the text for details).

X-ray sources are likely located.

The closest source (Src 11) to the Draco center is at distance of about $51''$, Src 67 [Src 3] at $76''$ [$51''$] from Leo I [UMa II] center (see Fig. 5). These distances are well above the source error boxes ($1.2''$, $0.7''$ and $1.4''$, respectively) so we infer that none of the high-energy sources is located at the center of these dSphs. Nevertheless, using the minimum unabsorbed fluxes and the distances reported by NED, we estimated an upper limit to the luminosity (in the 0.2-12.0 keV energy band) of the compact central object (if any), getting about 4.75×10^{33} erg s $^{-1}$, 1.21×10^{34} erg s $^{-1}$ and 1.05×10^{33} erg s $^{-1}$ for Draco, Leo I and UMa II, respectively.

Scaling the previous minimum fluxes to the 0.5-2.0 keV energy band, we obtained, via the logN-logS relation, the expected number of the background sources (within $25''$): $0.08^{+0.18}_{-0.03}$, $0.18^{+0.07}_{-0.06}$ and $0.06^{+0.10}_{-0.02}$, respectively. Being well below the unity, we infer that if any source exist in such a region, it should be located within the dwarf galaxies.

Despite any clear identification of central object, we also put an upper limit to the putative central BH mass (M_{BH}) by assuming it accretes through the Bondi-Hoyle spherical model. Bondi & Hoyle (1944) claimed that when a BH moves with velocity v through a gaseous medium, characterized by an hydrogen number density n , it accretes at a rate given by

$$\dot{M} \simeq \frac{4\pi(GM_{BH})^2 m_p n}{(v^2 + c_s^2)^{3/2}}, \quad (3)$$

where m_p is the proton mass and c_s the sound speed in the medium. Then, the subsequent X-ray luminosity $L_X \simeq \epsilon \eta \dot{M} c^2$ can be rewritten as

$$L_X \simeq \epsilon \eta 8.8 \times 10^{36} \left(\frac{M_{BH}}{10^3 M_\odot} \right)^2 \left(\frac{V}{15 \text{ km s}^{-1}} \right)^{-3} \left(\frac{n}{0.1 \text{ cm}^{-3}} \right) \text{ erg s}^{-1},$$

with $V = (v^2 + c_s^2)^{1/2}$, while ϵ is the efficiency in converting mass to radiant energy and η the fraction of the Bondi-Hoyle accretion rate onto the BH.

Assuming $v \simeq c_s \simeq 10 \text{ km s}^{-1}$ (consequently $V \simeq 15 \text{ km s}^{-1}$) and n in the range $10^{-3} - 10^{-1} \text{ cm}^{-3}$ as typical values for this kind of system, we obtain that the IMBHs (if any) at the center of these galaxies must have an upper limit mass of $\simeq 100 M_\odot$. Of course, this estimate scales as $(\epsilon \eta)^{-0.5}$. We also searched for radio sources in the NRAO VLA Sky Survey (NVSS) (within $100''$ from the dSph centers) with the aim of obtaining a better BH mass estimate. However, no radio source was found.

4.5 The case of UMi dSph

The possibility that UMi dSph hosts a BH in its center was already studied quite intensely. For example, Maccarone et al. (2005a) found a radio source within 3σ error box from the galaxy center and, assuming the existence of an accreting IMBH and a gas density as low as 1/30-1/100 of the typical density in globular clusters, these authors realized that a central black hole with mass of few $10^5 M_\odot$ would be necessary in order to explain the observed radio flux. Furthermore, Lora et al. (2009) inferred an upper limit of $2-3 \times 10^4 M_\odot$ using N-body simulations of the tidal disruption of a long lived substructure observed on the north-east side of the UMi major axis. It was also claimed that the compact object may not residing in the galactic center but offset from it because of gravitational effects.

Nucita et al. (2013b) analyzed the X-ray data acquired by the Chandra satellite for $\simeq 19.8$ ks in 2011 (Obs. id. 12754) and found an X-ray source (at J2000 coordinates RA = $15^h 09^m 14.37^s$ and Dec = $67^\circ 12' 58.4''$, with associated error of $\simeq 0.52''$) with an unabsorbed 0.5-7.0 keV flux of $F_{0.5-7.0 \text{ keV}}^{Unabs} \simeq 4.9 \times 10^{-15} \text{ erg s}^{-1}$. The X-ray source was spatially coincident (within $\simeq 1.2''$) with a source (the same already identified in the radio band by Maccarone et al. 2005a) with a flux density of $7.1 \pm 0.4 \text{ mJy}$ at 1.4 GHz. Such radio source 150914+671258 was detected by NRAO VLA Sky Survey (NVSS) at J2000 coordinates RA = $15^h 09^m 14.56^s$ and Dec = $67^\circ 12' 58.9''$ and the relevant positional error is $\simeq 2.1''$ as obtained from the sum in quadrature of the uncertainties associated to the two coordinates. Under the assumption that the observed

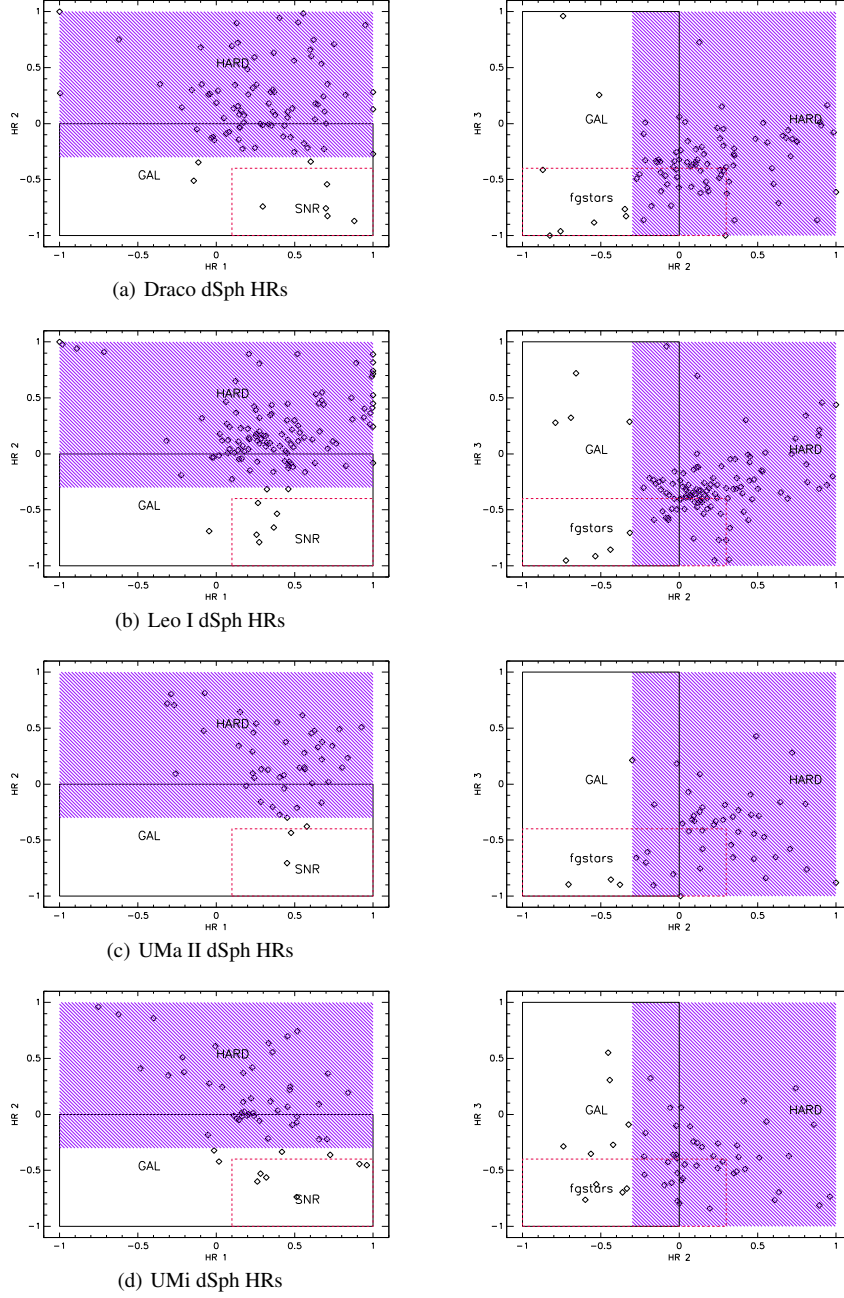


Figure 4. The HRs color-color diagram for our X-ray sources (see text for details).

source is an accreting IMBH, Nucita et al. (2013b) used the fundamental plane relation to evaluate the BH mass, which resulted to be $(2.9^{+33.6}_{-2.7}) \times 10^6 M_{\odot}$. As stressed by the same authors, the detection algorithm (*wavdetect*) was run with a significance threshold of 10^{-6} corresponding to the possibility to have at least one false detection in the CCD where the target is found. Hence, the source was detected by Chandra only at $\approx 2.5\sigma$ confidence level.

Here, in order to test the robustness of this result, we analyzed the 2005 *XMM-Newton* data and found that, as shown in Fig. 5(d), an X-ray source (Src 3) is clearly detected and superimposed to the location of the galaxy center. In particular, Src 3 (with J2000 coordinates $RA = 15^h 09^m 13.1^s$ and $Dec = 67^{\circ} 12' 59.4''$) has a distance of $\approx 30''$ from UMi center (white circle) as reported by

Falco et al. (1999)¹⁰, and a galactocentric distance $\approx 24''$ if the SIMBAD database coordinates¹¹ are considered. In the same Figure, we give the position of the X-ray source detected by Chandra (1'' red circle) and the associated NVSS radio counterpart (2'' magenta circle). Note that the distance between the *XMM-Newton* and Chandra sources is $\approx 7.4''$.

¹⁰ Falco et al. (1999) assigned a positional uncertainty of $\approx 3.5''$, obtained as a sum in quadrature of the errors ($\approx 2.5''$) associated on RA and Dec, to UMi galaxy center.

¹¹ UMi dSph is located, as reported by SIMBAD (yellow circle), at J2000 coordinates $RA = 15^h 09^m 11.34^s$ and $Dec = 67^{\circ} 12' 51.7''$ with a positional uncertainty of $\approx 12.2''$, due to the sum in quadrature of the RA ($\approx 2''$) and Dec ($\approx 12''$) errors.

(a) Draco dSph					(b) Leo I dSph				
Annulus	R_{in} (arcmin)	R_{ex} (arcmin)	# Exp	# Obs	Annulus	R_{in} (arcmin)	R_{ex} (arcmin)	# Exp	# Obs
1	0.00	0.76	0.2 ± 0.1	0	1	0.00	0.76	0.6 ± 0.1	0
2	0.76	3.60	5.6 ± 1.0	7	2	0.76	3.60	13.4 ± 2.2	11
3	3.60	6.50	13.3 ± 2.4	13	3	3.60	6.50	31.4 ± 5.0	26
4	6.50	9.00	17.6 ± 3.1	22	4	6.50	9.00	41.7 ± 6.8	25
5	9.00	16.00	79.4 ± 14.1	46	5	9.00	16.00	188.3 ± 30.7	53

(c) UMa II dSph					(d) UMi dSph				
Annulus	R_{in} (arcmin)	R_{ex} (arcmin)	# Exp	# Obs	Annulus	R_{in} (arcmin)	R_{ex} (arcmin)	# Exp	# Obs
1	0.00	0.76	0.2 ± 0.1	0	1	0.00	0.76	0.3 ± 0.1	1
2	0.76	3.60	4.5 ± 0.9	3	2	0.76	3.60	6.1 ± 1.8	5
3	3.60	6.50	10.9 ± 2.0	13	3	3.60	6.50	14.6 ± 4.3	10
4	6.50	9.00	14.4 ± 2.6	11	4	6.50	9.00	19.2 ± 5.6	12
5	9.00	16.00	65.1 ± 11.6	22	5	9.00	16.00	86.8 ± 25.4	26

Table 12. List of sources expected through the logN-logS diagram and observed in annuli around the galaxy centers of our sample. Here, R_{in} and R_{ex} represent the interior and exterior annulus radii, respectively.

Src 3 is characterized by an absorbed 0.2-12.0 keV flux of $7.3 \pm 2.9 \times 10^{-15} \text{ erg s}^{-1} \text{ cm}^{-2}$ which corresponds to an unabsorbed flux of $F_{0.2-12.0 \text{ keV}}^{Unabs} = (7.90 \pm 3.14) \times 10^{-15} \text{ erg s}^{-1} \text{ cm}^{-2}$. The unabsorbed 2-10 keV band flux is $F_{2-10 \text{ keV}}^{Unabs} = (4.05 \pm 1.61) \times 10^{-15} \text{ erg s}^{-1} \text{ cm}^{-2}$.

Assuming a distance of $73 \pm 10 \text{ kpc}$, as reported by NED, we are left with a luminosity $L_{0.2-12.0 \text{ keV}}^{Unabs} = (4.88 \pm 2.37) \times 10^{33} \text{ erg s}^{-1}$ and $L_{2-10 \text{ keV}}^{Unabs} = (2.50 \pm 1.21) \times 10^{33} \text{ erg s}^{-1}$.

Following Nucita et al. (2013b) and the references therein, we can get constraints on the possible central BH parameters. In fact, from the correlation between X-ray Src 3 and the radio 150914+671258 source (at distance of $\approx 3.6''$), we can estimate the BH mass using the fundamental plane relation (Merloni et al. 2003, K rding et al. 2006)

$$\log L_R = \xi_{RX} \log(L_X) + \xi_{RM} \log(M_{BH}) + b_R \quad (4)$$

where the mass and the luminosities are in units of solar masses M_\odot and erg s^{-1} , respectively, $\xi_{RX} = 0.60^{+0.11}_{-0.11}$, $\xi_{RM} = 0.78^{+0.11}_{-0.09}$ and $b_R = 7.33^{+4.05}_{-4.07}$. Solving for the black hole mass, Merloni et al. (2003) obtained

$$\log(M_{BH}) \approx 16.3 + \log(D) + 1.28 [(\log(F_R) - 0.60 \log(F_X))] \pm 1.06, \quad (5)$$

where D is the source distance expressed in Mpc and the last term is a consequence of the scatter in the fundamental plane relation.

From the 1.4 GHz radio flux density of the source 150914+671258, we obtained the 5 GHz one, assuming $F(\nu) \propto \nu^{-\alpha_R}$. So, assuming a flat source spectrum ($\alpha_R \approx 0$), we get $F(5 \text{ GHz}) \approx 7.1 \text{ mJy}$, consequently a radio flux $F_R = (3.5 \pm 0.2) \times 10^{-16} \text{ erg cm}^{-2} \text{ s}^{-1}$ and a radio luminosity of $L_R = (2.19 \pm 0.62) \times 10^{32} \text{ erg s}^{-1}$.

Using the previous estimate of the radio (5 GHz) and X-ray (2-10 keV) fluxes in eq. (5), we estimate a mass of $(2.76^{+32.00}_{-2.54}) \times 10^6 M_\odot$ for the putative IMBH. The rather large uncertainty is mostly due to the intrinsic scatter of the fundamental plane relation. The obtained IMBH mass is consistent with that estimated by Nucita et al. (2013b) when analyzing the 2011 Chandra data. We also note that this result slightly depends on the index α_R of the radio spec-

tral energy distribution. Changing α_R , M_{BH} scales with the factor $(1.4 \text{ GHz}/5 \text{ GHz})^{1.28\alpha_R}$. For example, for $\alpha_R \approx 0.4$ the BH mass gets reduced by $\approx 50\%$.

Note also that when scaling the 0.2-12 keV source flux (as detected by the XMM-Newton) to the range 0.5-7 keV, one gets a flux consistent (within the errors) to that estimated using the 2011 Chandra data. The corresponding 0.5-7.0 keV luminosity is $L_X = L_{0.5-7.0 \text{ keV}} = (3.21 \pm 2.17) \times 10^{33} \text{ erg s}^{-1}$. By comparing the bolometric luminosity, calculated as $L_B \approx 16L_X$ (Ho 2008), with the expected Eddington one $L_{Edd} \approx 1.3 \times 10^{38} (M_{BH}/M_\odot) \text{ erg s}^{-1}$, one gets $L_B/L_{Edd} \approx 1.43 \times 10^{-10}$. This clearly shows that the UMi putative BH is radiatively inefficient. Indeed, assuming the simplified Bondi accretion scenario, we use eq. (4) with $L_X = L_{0.2-12.0 \text{ keV}}^{Unabs}$ and obtain

$$\epsilon \eta \approx 7.3 \times 10^{-11} - 7.3 \times 10^{-9}, \quad (6)$$

that confirms the expected low IMBH accretion efficiency, previously highlighted.

Finally, we evaluate the expected number of background objects to investigate the possibility that the high energy emission of Src 3 is due to an object standing behind. By using the minimum X-ray detected flux towards UMi, correctly scaled to the 0.5-2.0 keV band ($F_{0.5-2.0 \text{ keV}}^{Una} \approx 1.80 \times 10^{-15} \text{ erg s}^{-1} \text{ cm}^{-2}$), we get $N \approx 0.07$ within $25''$ from the center. In spite of the small value of N , the background scenario cannot be definitively ruled out.

5 CONCLUSIONS

In this paper, we re-analyzed some deep archival XMM-Newton data sets in order to full characterize the high-energy point-like source population of four dSph MW companions. Hence, the ultimate goal, is to classify the X-ray sources identified towards our galaxy sample and pinpoint local (or candidate local) sources.

We performed an accurate study obtaining 89 X-ray sources for Draco, 116 for Leo I, 49 for UMa II and 54 for UMi. Albeit these values are statistically consistent with those of background AGNs, theoretically reached via the logN-logS relation, we cannot

rule out the possibility that some sources belong to the same dSphs. This claim is supported by the color-color diagram (based on the ratio between 0.2 – 2.4 keV X-ray and J band NIR fluxes versus the J-K color). In this way we find that some X-ray sources, correlating with counterparts in the 2MASS catalogue, have a stellar nature (see Fig. 3 and Sect. 4.1). Further, we perform a statistical source sorting using only the high-energy data. This leads us to a wider and more complete classification of the X-ray sources in the target field of view. We reveal two high-energy sources (among which a carbon star) belonging to Draco, one to UMa II and none to Leo I. Although the the statistic at our hand is poor, finding a few possible local X-ray sources may represent a problem that need to be addressed. In fact, dSph galaxies, as globular clusters, host mainly old star populations but, due to the much lower central stellar density in dSphs, X-ray sources (either LMXBs or CVs) are expected to be primordial objects and not formed by capture encounters. However, these X-ray sources, should already turned off making unlikely to being found in dSphs. Finding X-ray sources in dSphs represent therefore a puzzling problem and in any case may allow to test the formation theories of these objects in a contrasting environment with respect to that in globular clusters..

By extrapolating the fundamental $M_{BH} - M_{Bulge}$ relation to the dSph realm, one sees that these galaxies are expected to contain IMBHs in their gravitational centers. We thus searched for X-ray sources located within the core radius of the dSphs of our sample. However, for Draco, Leo, and UMa we did not identify any high-energy (and radio) sources nearby the galactic centers. Then, we can only put upper limits to the mass and luminosity of the putative central IMBHs.

On the contrary, it is interesting that the UMi center hosts an X-ray source –Src 3– which correlates in position with a radio object. In the IMBH hypothesis, the fundamental plane relation of eq. (5) allows us to get an estimate of the mass (a few $10^6 M_\odot$) of the accreting black hole possible hosted in the galaxy. We remind that the source was already detected by Chandra in the past but only at the poor $\approx 2.5\sigma$ confidence level, thus leaving the possibility that the Chandra source was a mere fake detection.

Our analysis, based on independent *XMM*-Newton data, confirms however Src 3 as a possible X-ray counterpart of an accreting IMBH.

ACKNOWLEDGMENTS

We thank M. Guainazzi for stimulating discussions while preparing the manuscript. We also acknowledge the support by the INFN project TaSP. We thank the anonymous Referee for the suggestions that greatly improved the paper. One of us (AAN) is grateful to Matteo Nucita for reading the draft.

REFERENCES

- Arnaud K. A., 1996, in Jacoby G., Barnes J., eds, *Astronomy Society of the Pacific Conference Series Vol. 101, XSPEC: The First Ten Years*, in *Astronomical Data Analysis Software and Systems V*, Astron. Soc. Pac., San Francisco, p. 17
- Assmann, P., Fellhauer, M., Wilkinson, M. I., Smith, R., 2013a, *MNRAS*, 432, 274A
- Assmann, P., Fellhauer, M., Wilkinson, M. I., Smith, R., Blańa, M., 2013b, *MNRAS*, 435, 2391A
- Baade, W., Swope, H. H., *Astronomical Journal*, 1961, 66, 300
- Bartlett, E. S., Coe, M. J., Haberl, F., McBride, V. A., Corbet, R. H. D., 2012, *MNRAS*, 422, 2302
- Bellazzini M., Ferraro F. R., Origlia L., Pancino E., Monaco L., Oliva E., 2002, *AJ*, 124, 3222
- Bonanos, A. Z., Stanek, K. Z., Szentgyorgyi, A. H., Sasselov, D. D., Bakos, G. Á., 2004, *AJ*, 127, 861
- Bondi, H., Hoyle, F., 1944, *MNRAS*, 104, 273
- Breddels, M. A., and Helmi, A., 2013, *A&A* 558, A35
- Bukhmastova, Yu. L., 2001, *Astron. Rep.*, 45, 581
- Carrera, R., Aparicio, A., Martínez-Delgado, D., Alonso-García, J., 2002, *AJ*, 123, 3199C
- Casas, R. A., Arias, V., Peña Ramírez, K., Kroupa, P., 2012, *MNRAS*, 424, 1941C
- Cavuoti, S., Brescia M., D’Abrusco R., Longo G., Paolillo M., 2014, *MNRAS*, 437, 968
- Cioni, M. R. L., Habing, H. J., 2005, *A&A*, 442, 165
- D’Abrusco, R., Longo, G., Walton, N. A., 2009, *MNRAS*, 396, 223
- Dall’Ora, M., et al., 2003, *AJ*, 126, 197
- Dall’Ora M. et al., 2012, *ApJ*, 752, 42
- de la Calle I. et al., eds, 2014, *XMM-Newton Proposers Guide and Phase II Remote Proposal System Users Manual*, issue 14.0 (ESA: XMM-Newton SOC)
- Dehnen, W., & King, A., 2006, *MNRAS*, 367, 29
- Falco, E. E., Kurtz, M. J., Geller, M. J., et al., 1999, *PASP*, 111, 438
- Fellhauer, M., et al., 2007, *MNRAS*, 375, 1171
- Ferrarese, L., Merrit, D., 2000, *ApJ*, 539, L9
- Flesch, E., 2010, *PASA*, 27, 283
- Jardel, J. R., & Gebhardt, K., 2012, *ApJ*, 746, 89
- Gebhardt, K., et al., 2000, *ApJ*, 539, L13
- Goranskij, V. P., 1982, *Astronomicheskii Tsirkulyar* NO.1216
- Grillmair, C. J., Mould, J. R., Holtzman, J. A., et al., 1998, *AJ*, 115, 144
- Guainazzi, M., 2010, *XMM-SOC-CAL-TN-0018*, *XMM-Newton Science Operations Centres* <http://xmm2.esac.esa.int/docs/documents/CAL-TN-0018.ps.gz>
- Gullieuszik, M., Held, E. V., Saviane, I., Rizzi, L., 2009, *A&A*, 500, 735
- Haakonsen, C. B., Rutledge, R. E., 2009, *ApJS*, 184, 138
- Harrington, R. G., Wilson, A. G., 1950, *PASP*, 62, 365, 118
- Harris, W.E., 1996, *AJ*, 112, 1487
- Hasinger, G., Miyaji, T., Schmidt, M., 2005, *A&A*, 441, 417
- Held E. V., Gullieuszik M., Rizzi L., Girardi L., Marigo P., Saviane I., 2010, *MNRAS*, 404, 1475
- Ho, L. C., 2008, *A&A*, 46, 475
- Ibata, R., Irwin, M., Lewis, G. F., Stolte, A., 2001, *ApJ*, 547, L133
- Kinemuchi, K., Smith, H. A., Lacluzé, A. P., et al., 2002, *Radiation and Nonradial Pulsations as Probes of Stellar Physics*, ASP Conference Proceedings, 259, Edited by Conny Aerts, Timothy R. Bedding, and Jørgen Christensen-Dalsgaard. ISBN: 1-58381-099-4. Also IAU Colloquium 185. San Francisco: Astronomical Society of the Pacific, 130
- Kinemuchi K., Harris H. C., Smith H. A., Silbermann N. A., Snyder L. A., La Cluzé A. P., Clark C. L., 2008, *ApJ*, 136, 1921
- Kirsch, M. G. F., et al., 2004, in *Proc. SPIE*, 5488, 103
- Koch A., Wilkinson M. I., Kleyna J. T., Gilmore G. F., Grebel E. K., Mackey A. D., Evans N. W., Wyse R. F. G., 2007, *ApJ*, 657, 241
- Körding, E., Falcke, H., Corbel, S., 2006, *A&A*, 456, 439
- Lemons, S.M., Reines, A. E., Plotkin, R. M., Gallo, E., & Greene,

- J.E., 2015, e-print arXiv:1502.06958
- Lora, V., Sánchez-Salcedo, F. J., Raga, A. C., Esquivel, A., 2009, ApJ, 699, L113
- Maccarone, T. J., Fender, R. P., Tzioumis, A. K., 2005a, Astrophys. Space Sci., 300, 239
- Maccarone, T. J., Kundu, A., Zepf, S. E., Piro, A. L., Bildsten, L., 2005b, MNRAS, 364, L61
- Magorrian, J., Tremaine, S., Richstone, D., 1998, AJ, 115, 2285
- Majewski, S. R., Ostheimer, J. C., Patterson, R. J., et al., 2000, AJ, 119, 760
- Malyshev, D., Neronov, A., & Eckert, D., 2014, Phys. Rev. D, 90, 103506
- Martin, N. F., de Jong, J. T. A., Rix, H.-W., 2008, ApJ, 684, 1075
- Martínez-Delgado, D., Alonso-García, J., Aparicio, A., Gómez-Flechoso, M. A., 2001, ApJ, 549, L63
- Mateo, M., 1997, in Arnaboldi M., Da Costa G. S., Saha P., eds, Astronomical Society of the Pacific Conference Series Vol. 116, The Nature of Elliptical Galaxies. Astron. Soc. Pac., San Francisco, p. 259
- Mateo, M., Olszewski, E. W., Morrison, H. L., 1998, ApJ, 508, L55
- McConnachie, A. W., 2012, AJ, 144, 4
- Menzies, J. W., Whitelock, P. A., Feast, M. W., Matsunaga, N., 2010, MNRAS, 406, 86
- Merloni, A., Heinz, S., Di Matteo, T., 2003, MNRAS, 345, 1057
- Monet, D. G., Levine, S. E., Canzian, B., 2003, AJ, 125, 984
- Muñoz, R. R., Geha, M., Willman, B., 2010, AJ, 140, 138
- Nemec, J. M., AJ, 1985, 90, 204
- Nucita, A. A., Manni, L., De Paolis, F., Vetrugno, D., Ingrosso, G., 2013a, A&A, 550, 18
- Nucita, A. A., De Paolis, F., Manni, L., Ingrosso, G., 2013b, New Ast., 23, 107
- Odenkirchen, M., et al., 2001, ApJ, 122, 2538
- Ofek, E. O., et al., 2012, PASP, 124, 854
- Orio M., Gallagher J., Greco C., Held E., Walker N. H., Pavan L., 2010, AIP Conf. Proc., 1314, 337
- Pietsch, W., Misanovic, Z., Haberl, D., Ehle, M., Trinchieri, G., 2004, A&A, 426, 11
- Podsiadlowski Ph., Rappaport S., Pfahle E., Han Z., Beer M. E., 2004, in Rasio F. A., Stairs I. H., eds, Astronomy Society of the Pacific Conference Series Vol. 328, Binary Radio Pulsars. Astron. Soc. Pac., San Francisco, p. 327
- Ramsay, G., Wu, K., 2006, A&A, 459, 777
- Rave H. A., Zhao C., Newberg H. J., Yanny B., Schneider D. P., Brinkman J., Lamb D. Q., 2003, ApJS, 145, 245
- Reines, A. E., Greene, J. E., Geha, M., 2013, ApJ, 775, 116
- Richards, G. T., et al., 2010, ApJ S, 180, 67
- Roeser S., Schilbach E., Schwan H., Kharchenko N. V., Piskunov A. E., Scholz R. D., 2008, A&A, 488, 401
- Roeser, S., Demleitner, M., Schilbach, E., 2010, AJ, 139, 2440
- Silk, J., Wyse, R. F. G., Shields, G. A., 1987, ApJ, 322, 59
- Skrutskie, M. F., et al., 2006, AJ, 131, 1163
- Smecker-Hane, T. A., Marsteller, B., Cole, A., Bullock, J., Gallagher, J. S., 2009, Bulletin of the American Astronomical Society, 41, 235
- Smith R., Fellhauer M., Candlish G. N., Wojtak R., Farias J. P., Blana M., 2013, MNRAS, 433, 2529
- Stetson, P. B., Hesser, J. E., & Smecker-Hane, T. A. 1998, PASP, 110, 533
- Walker, M. G., Mateo, M., Olszewski, E. W., 2007, ApJ, 667, L53
- Watson, M. G., et al., 2009, A&A, 493, 339
- Wilson, A. G., PASP, 1955, 67, No. 394, 27
- Yang, Y., Hammer, F., Fouquet, S., et al., 2014, e-print arXiv:1405.2071
- Zinn, R., Searle, L., 1976, ApJ, 209, 734
- Zucker, D. B., Belokurov, V., Evans, N. W., et al., 2006, ApJ, 650, L41

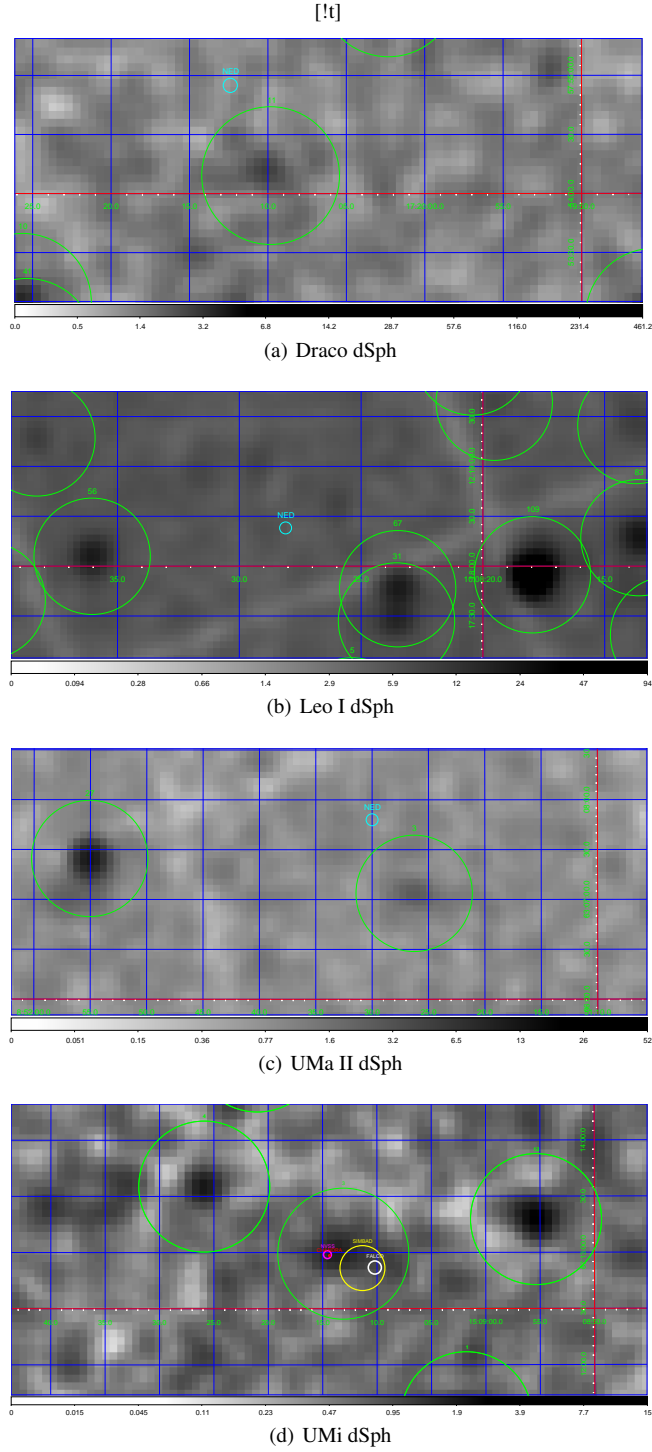


Figure 5. Zoom view of the four dSph centers. In the last panel, the green, red and magenta circles represent the position of the X-ray source identified at the center of UMi and its counterparts for Chandra and NVSS, respectively. The yellow and white circles show the centers of the galaxy as reported in Falco et al. (1999) and SIMBAD database.